ISSN 2277-2685
IJPSL/Dec. 2023/ Vol-13/Issue-4/33-49
Hanumanthu, *et. al* International Journal of Pharmacetical Sciences Letters

Antiproliferative Effect of 7-Ketositosterol in Breast and Liver Cancer Cells: Possible Impact on Ceramide, Extracellular Signal-Regulated Kinases, and Nuclear Factor Kappa B Signaling Pathways

Hanumanthu 1, S.Umarani 2, K.Anand Kumar 3, K.Ganesh 4,

Assistant professor 1,2,3,4 Department of Pharmacy, Samskruti College of Pharmacy, Kondapur (V), Ghatkesar (M) Medchal Dist, Telangana, India

A. Article Info

Received: 20-04-2023 ***Revised: 25 -07-2023*** ***Accepted: 20-08-2023***

Abstract: 7-Ketositosterol (7-KSS) was the focus of this investigation because of its potential effects on sphingomyelin/ceramide metabolites and cell death in HepG2 and MCF-7 human liver cancer cells. Methods: At various concentrations and times, the anti-proliferative effects of 7-KSS therapy were evaluated. Cell viability was determined by MTT analysis, while sphingomyelins (SMs), ceramides (CERs), and sphingosine-1-phosphate (S1P) levels were analyzed by LC-MS/MS. Western blot analysis and immunofluorescence labeling were used to determine the amounts of phosphorylated 44/42 ERK1/2 and NF-κB p65 (Ser536) proteins. The process of cell death was examined by using flow cytometric analysis of annexin-V and propidium iodide (PI) labeling, as well as TUNEL staining. In comparison to control cells, 7-KSS treatment considerably reduced cell viability and levels of S1P, p-44/42 ERK1/2, and p-NF-κB p65 proteins in cancer cells. In cancer cells treated with 7-KSS, apoptosis and intracellular levels of C16-C24 CERs were shown to increase significantly. Results: S1P, p-44/42 ERK1/2, and p-NF-κB p65 protein levels were downregulated by 7-KSS, which decreased cell proliferation and increased ceramide buildup and apoptosis.

Keywords: 7-Ketositosterol; ceramide; apoptosis; ERK

1. Introduction

Recent studies have indicated that dietary plant sterols may protect against many types of cancer [1,2]. The natural compound 7-ketositosterol comes from phytosterols, which are oxidized plant sterols [3]. It is well-known that phytosterols, which look like cholesterol, may help reduce human cholesterol levels by preventing the intestinal absorption of cholesterol [4]. One of the most common phytosterols found in plants, including nuts, seeds, fruits, and vegetables, is beta-sitosterol. One common dietary supplement for cholesterol management is beta-sitosterol, which is well-known for its ability to decrease cholesterol levels [5]. Many plant oils, seeds, and nuts also contain campesterol, another kind of phytosterol. Campesterol, like beta-sitosterol, may reduce cholesterol levels [6]. You may find stigmasterol in a variety of foods, including beans, vegetables, and grains. Because of its structural similarity to cholesterol, stigmasterol has been

effects. More study is required in this area, however there is some indication that phytosterols may affect immunological function [6]. Phytosterols have anti-inflammatory characteristics, according to some research [7]. This means they might help with inflammatory disorders including arthritis and cardiovascular disease. The antioxidant properties of phytosterols may aid in the neutralization of free radicals and the reduction of oxidative stress, two factors that contribute to a number of illnesses and the aging process [7]. Due to their structural similarity to cholesterol and their potential to decrease the risk of certain cancers through multiple mechanisms, including reducing inflammation, modulating immune responses, or interfering with cancer cell growth pathways, phytosterols have garnered some interest in the context of cancer [8]. Prompting cell cycle arrest, regulating oxidative stress, enhancing metabolic reprogramming, thwarting drug resistance, modifying immunology and inflammation, and inducing apoptosis are all mechanisms by which beta-sitosterol has been associated with its anticancer effects [9]. In relation to cell death, β-sitosterol exerts its effects via many mechanisms. As an example, β-sitosterol changes components like p21 and p53 to regulate p53, which in turn causes apoptosis in A549 lung cancer cells [10]. Interactions with Bcl-2, pro-caspase-3, and Bax are known to cause apoptosis in gastric cancer [10]. Similarly, HepG2 cells activate internal and extrinsic apoptotic pathways, which include death receptors and Bcl-2 [10]. There are many mechanisms via which β-sitosterol affects cell cycle arrest. By inhibiting Cyclin-D1 and cyclin-dependent kinase 2 (CDK-2), β-sitosterol causes cell cycle arrest in lung adenocarcinoma, as an example [10]. When it comes to cancer migration, β-sitosterol mostly operates via the signaling pathways of epithelial-mesenchymal transition (EMT) and protein kinase B/glycogen synthase kinase 3 beta (AKT/GSK-3b) [10]. Phytosterols are vulnerable to oxidation because their chemical structure contains two links [11]. The creation of phytosterol oxidation products (POPs) [11] may occur when free radicals remove hydrogen atoms from both links. By promoting the formation of reactive oxygen species, transition metal ions like copper and iron may accelerate the oxidation of phytosterols. Phytosterols may be more easily oxidized when exposed to light, especially ultraviolet (UV) radiation [12]. Hydroperoxides, epoxidides, aldehydes, and ketones are among the oxidation products that may be formed when phytosterols are oxidized [11]. It is possible that the chemical characteristics and biological activity of these oxidized phytosterols are different from those of their unoxidized counterparts [13]. Also, it's possible for some oxidation products to cause cell death [14,15]. When beta-sitosterol undergoes oxidation, it produces 7-ketoestrol. There have been reports that it is the most prevalent POP in commercial spreads [16]. According to earlier research, 7-KSS has cytotoxic and apoptotic effects on human HepG2 liver cancer cells [14]. Phytosterols increase ceramide levels in cancer cells of the breast, colon, and prostate in humans [17]. Cancer cells undergo apoptosis when ceramide levels rise, which inhibits cell growth and activates caspases [18]. Extracellular signal-regulated kinases (ERKs), sometimes called mitogen-activated protein

A key role in cancer development is played by mitogen-activated protein kinases (MAPKs) [19]. It is well-established that phytoster-ols regulate ERK signaling [20]. Ceramide is also known to inhibit ERKs, which are composed of ERK1 and ERK2 [21]. Activated protein 1 (AP1) signaling pathway stimulation of the extracellular signal-regulated kinase (ERK) proteins occurs when toll-like receptor 4 (TLR4) upstream acts as an input [22]. According to [23], ERKs and nuclear factor kappa B (NF-κB) manage the expression of genes involved in the cell cycle, leading to an upregulation of cell growth, proliferation, and angiogenesis. By halting the activation of NF-κB and ERK signaling and the generation of cytokines, some phytosterols reduce the tumor microenvironment and decrease tumor development [20]. Unfortunately, 7-KSS is not as well-known or understood as other comparable chemicals, and its biological importance is still a subject of investigation. Here, we measured intracellular sphingolipid metabolite levels and apoptosis in human breast (MCF-7) and liver (HepG2) cancer cells to determine 7-KSS's anti-proliferative and anticancer effectiveness. Both cancer cell lines express TLR-4, according to studies [24,25]. That being said,

also determined the impact of 7-KSS on ERK signaling pathway downstream effectors by measuring phospho-NF-κB and phospho-ERK protein levels. In this study, we provide evidence that 7-KSS may reduce cell growth, induce apoptosis, and raise ceramide levels in human breast and liver cancer cells via preventing the phosphorylation of ERKs and NF-κB.

2. Results

2.1. Cell Viability Analysis

Viability analysis following 24 h 7-KSS treatment was performed in cancer cells and non-cancerous BJ fibroblasts (Figure 1). Treatment of MCF-7 cells with 5, 10, or 15 μM 7-KSS did not significantly affect cell viability over time. It was observed that 30 μM 7-KSS application significantly reduced cell viability in breast cancer cells by approximately 30% in 24 h (Figure 1A). Incubation of liver cancer cells with 5–30 μM 7-KSS for 12–18 h did not significantly affect cell viability compared to control and DMSO groups (Figure 1B). HepG2 cell viability was reduced significantly by approximately 25% after 24 h of 30 μM 7-KSS treatment. It was determined that 5–30 μM 7-KSS administration in the non-cancerous BJ fibroblast cell line did not significantly affect cell viability at 24 h (Figure 1C).

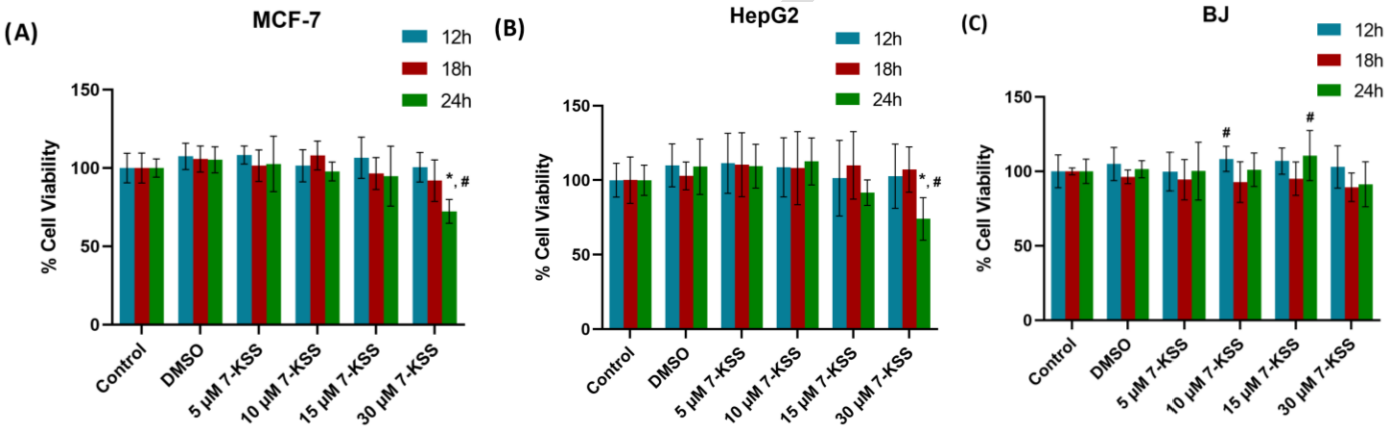

Figure 1. Examination of the carcinogenic effects of 7-ketositosterol on cancer cells and BJ fibroblasts. (A) Assessment of MCF-7 cell viability after 24 hours of 7-KSS treatment. The values are averages with standard deviations (n = 8). Statistical testing was carried out using either Kruskal-Wallis or one-way ANOVA. Tukey or Dunn's test was used to assess the difference between the groups. *, with a p-value less than 0.05, when compared to the control, DMSO, and 5 μM 7-KSS groups concurrently. **, $p < 0.05$ when contrasted with 12 h and 18 h within the same dosage period. (B) HepG2 cell viability analysis after 24 hours of 7-KSS treatment. The values are averages with standard deviations (n = 8). Statistical testing was carried out using either Kruskal-Wallis or one-way ANOVA. Tukey or Dunn's test was used to assess the difference between the groups. *, with a p-value less than 0.05, as compared to the control group, DMSO, 5 μM 7-KSS, and 10 μM 7-KSS at the specific time intervals. relative to 12 and 18 hours in the same dosage range, with a p-value less than 0.05.
(C) Evaluation of the vitality of 7-KSS in BJ fibroblast cells after 24 hours of treatment. Mean values plus or minus standard deviation (n = 7-8). Statistical testing was carried out using either Kruskal-Wallis or one-way ANOVA. Tukey or Dunn's test was used to assess the difference among the groups. 18 hours at the same dosage compared to #, $p < 0.05$.

2.2. Proliferating Cell Nuclear Antigen Levels

Figures 2A and 3A show PCNA immunofluorescence staining in MCF-7 and HepG2 cells incubated with 30 μM 7-KSS for 24 h. Quantitation of PCNA fluorescence staining showed that PCNA protein was significantly suppressed in MCF-7 cells (Figure 2D) and HepG2 cells (Figure 3D) treated with 7-KSS compared to control and DMSO groups. ELISA analysis of PCNA protein levels in MCF-7 (Figure 2E) and HepG2 (Figure 3E) cells confirmed immunofluorescence staining and showed that the amount of PCNA protein was meaningfully reduced in cancer cells incubated with 30 μM 7-KSS for 24 h vs. control and DMSO groups.

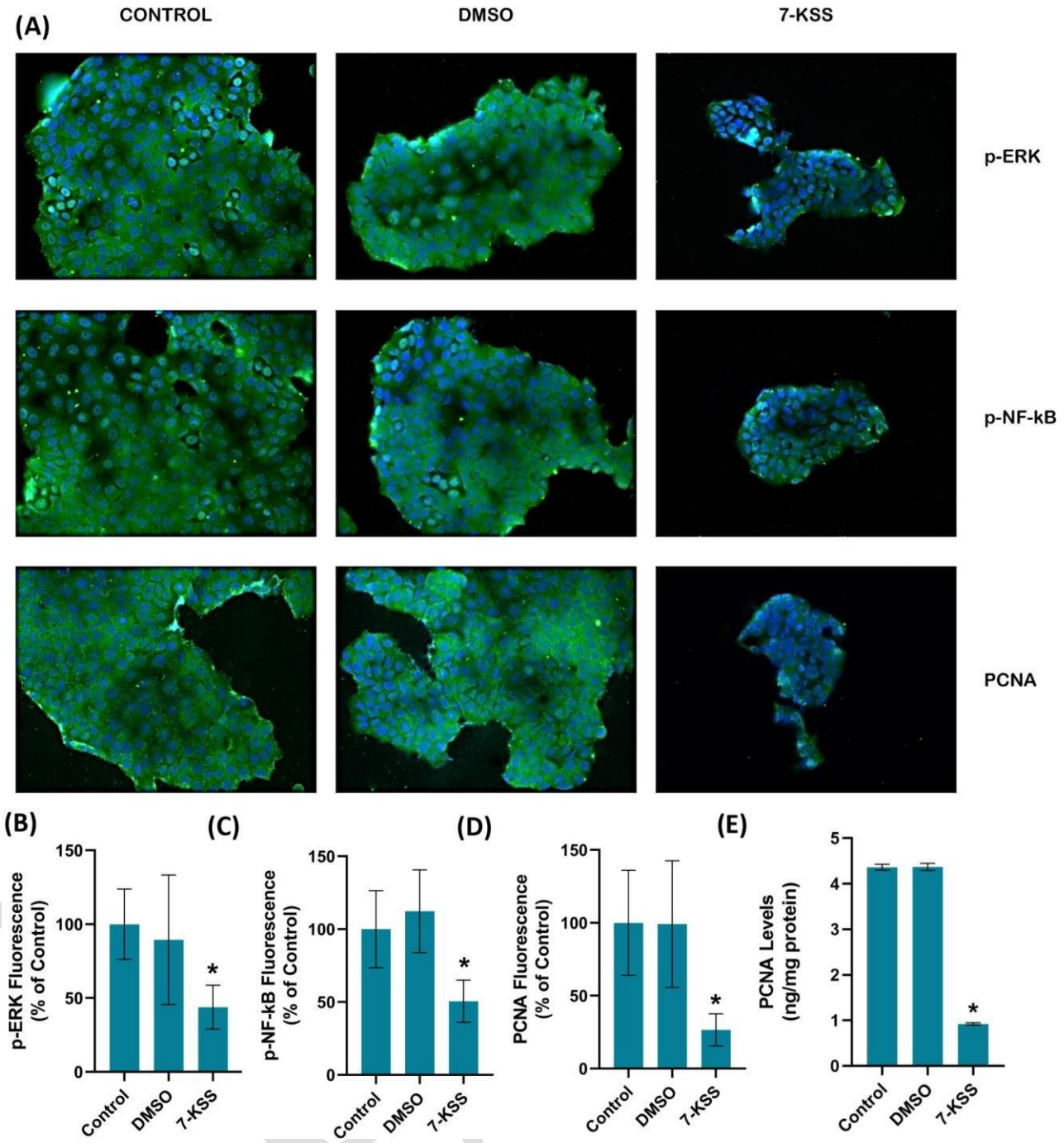

Figure 2. (**A**) Representative Immunofluorescent staining of p-ERKs, p-NF-κB, and PCNA in MCF-7 cells incubated with 30 μM 7-Ketositosterol for 24h. A 40× objective lens was used to obtain double-labeled images. (**B**) Quantitation of p-ERK fluorescence staining by ImageJ software. Values mean ± SD (n = 10). Kruskal–Wallis test and Dunn's multiple comparison analysis were performed to test statistical significance. * $p < 0.05$ vs. control and DMSO groups. (**C**) Quantitation of p-NF-κB fluorescence staining. Values are given as mean ± SD (n = 10). One-way ANOVA test and Tukey's multiple comparisons were used to determine statistical significance. * $p < 0.05$ compared to control and DMSO. (**D**) PCNA staining quantitation. Values are given as mean ± SD (n = 10). One-way ANOVA test and Tukey's multiple comparisons were used to determine statistical significance. * $p < 0.05$ compared to control and DMSO. (**E**) PCNA levels in MCF-7 cells. Values mean ± SD (n = 5). *, $p < 0.05$ vs. control and DMSO groups.

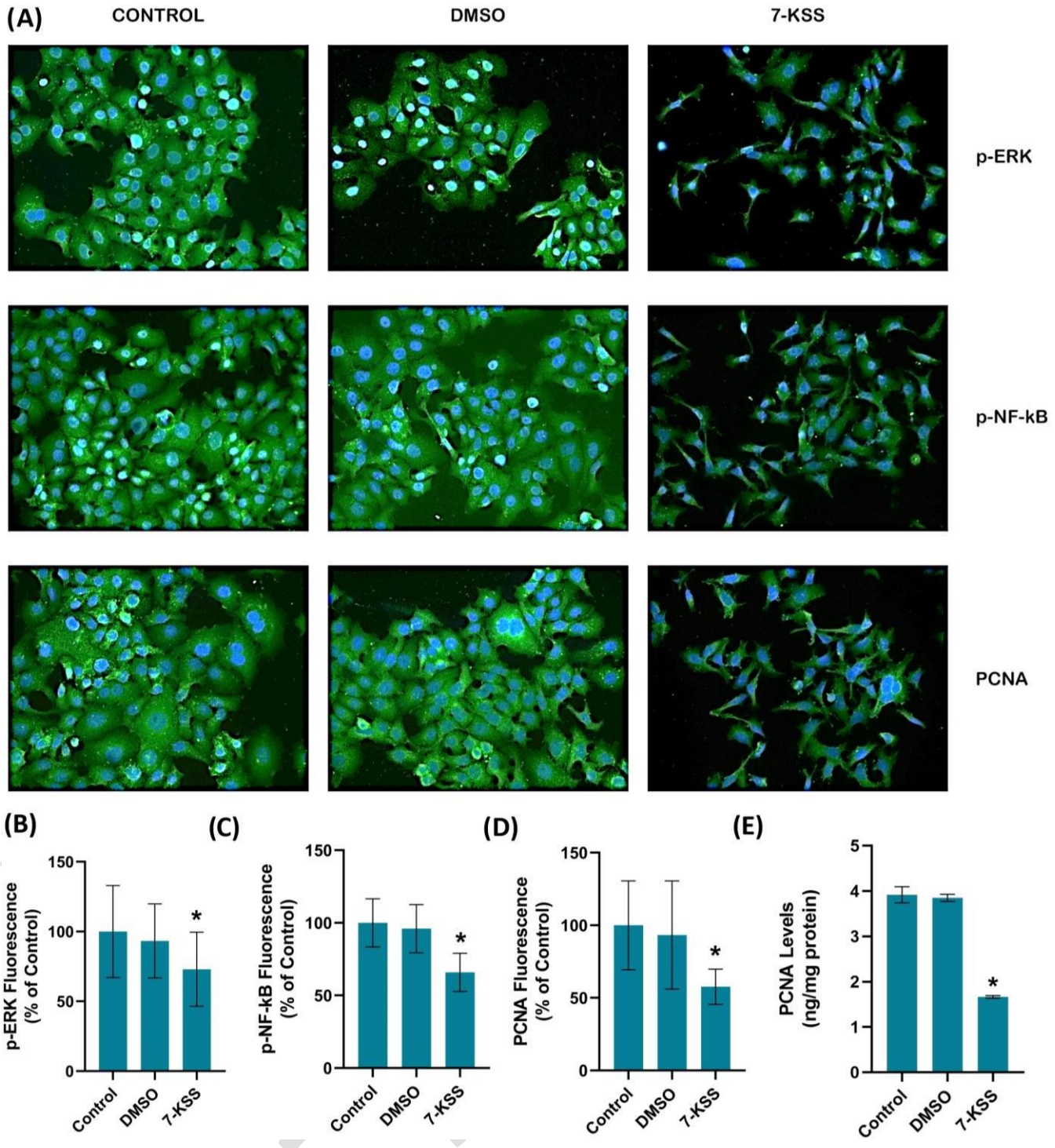

Figure 3. (**A**) Representative immunofluorescent staining of p-ERKs, p-NF-κB, and PCNA in HepG2 cells incubated with 30 μM 7-Ketositosterol for 24 h. A 40× objective lens was used to obtain double-labeled images. (**B**) Quantitation of p-ERK fluorescence staining by ImageJ software. Values mean ± SD (n = 10). Kruskal–Wallis test and Dunn's multiple comparison analysis were performed to test statistical significance. * $p < 0.05$ vs. control group. (**C**) Quantitation of p-NF-κB fluorescence staining. Values are given as mean ± SD (n = 10). One-way ANOVA test and Tukey's multiple comparisons analysis were used for statistical analysis. * $p < 0.05$ compared to control and DMSO groups. (C) Quantitation of PCNA fluorescence staining by ImageJ software. Values mean ± SD (n = 10). Kruskal–Wallis test and Dunn's multiple comparison analysis were performed to test statistical significance. * $p < 0.05$ vs. control and DMSO groups. (**E**) PCNA levels in HepG2 cell groups. Values mean ± SD (n = 5). One-way ANOVA and Tukey multiple comparison test were performed for statistical analysis. *, $p < 0.05$ vs. control and DMSO groups.

2.3. Sphingolipid Levels

Sphingolipid levels measured in cancer cells are shown in Table 1. A meaningful rise was detected in endogenous C18-C24 CERs levels in MCF-7 and HepG2 cells treated with 30 μM 7-KSS for 24 h, compared to control and DMSO groups. Incubation with 30 μM 7-KSS for 24 h considerably reduced S1P levels in cancer cells.

Table 1. Sphingolipid levels in cancer cells. All values mean ± SD. SM, sphingomyelin; S1P, sphingosine-1-phosphate; 7-KSS, 7-Ketositosterol. Statistical analysis was carried out by One-Way Analysis of Variance and all pairwise multiple comparison procedures were performed by the Tukey test. *, $p < 0{,}001$ vs. Control and DMSO groups.

	CONTROL	DMSO	7-KSS
Sphingolipids (ng/mg protein)			
16:0 SM (d18:1/16:0)			
MCF-7	159.83 ± 17.60	138.13 ± 21.36	143.80 ± 3.02
HepG2	154.40 ± 32.80	155.26 ± 27.77	178.63 ± 16.61
18:0 SM (d18:1/18:0)			
MCF-7	81.89 ± 8.14	84.93 ± 0.58	87.80 ± 9.12
HepG2	84.35 ± 6.49	89.53 ± 3.37	82.79 ± 5.70
24:0 SM (d18:1/24:0)			
MCF-7	34.51 ± 2.21	40.57 ± 7.38	39.94 ± 9.20
HepG2	40.38 ± 6.35	35.61 ± 5.96	39.22 ± 6.12
C16 Ceramide (d18:1/16:0)			
MCF-7	65.47 ± 7.88	65.89 ± 10.02	67.65 ± 2.76
HepG2	66.52 ± 8.58	66.20 ± 10.48	64.92 ± 8.75
C18 Ceramide (d18:1/18:0)			
MCF-7	7.40 ± 0.30	6.87 ± 0.71	37.20 ± 1.86 *
HepG2	6.26 ± 0.29	6.22 ± 0.16	34.89 ± 1.72 *
C20 Ceramide (d18:1/20:0)			
MCF-7	7.95 ± 0.27	7.60 ± 0.22	45.70 ± 2.67 *
HepG2	6.37 ± 0.18	6.54 ± 0.34	31.56 ± 0.52 *
C22 Ceramide (d18:1/22:0)			
MCF-7	24.11 ± 3.10	23.84 ± 4.22	64.63 ± 3.48 *
HepG2	23.97 ± 3.30	24.08 ± 3.04	66.50 ± 2.79 *
C24 Ceramide (d18:1/24:0)			
MCF-7	44.02 ± 2.48	43.20 ± 0.62	121.34 ± 13.16 *
HepG2	42.47 ± 5.03	35.30 ± 3.69	101.38 ± 1.77 *
S1P			
MCF-7	5.36 ± 0.27	5.00 ± 0.52	1.79 ± 0.08 *
HepG2	8.39 ± 0.27	7.92 ± 0.47	2.58 ± 0.15 *

2.4. Phospho-ERK and Phospho-NF-κB p65 Protein Levels

Immunofluorescent labeling of p-ERKs and p-NF-κB in HepG2 and MCF-7 cells treated with 30 μM 7-KSS for 24 hours is shown in Figures 2A and 3A. The phosphorylated proteins were shown to be considerably reduced in MCF-7 cells (Figure 2B,C) and HepG2 cells (Figure 3B,C) treated with 7- KSS, as compared to the control and DMSO groups, according to the quantitation of p-ERK and p-NF-κB fluorescence labeling. Figure 4A shows that immunofluorescence labeling of p-ERKs and p-NF-κB in cancer cells was also validated by Western blot analysis. There was agreement between the immunofluorescence results (Figure 4B-E) and the significantly reduced p-ERK/Total ERK and p-NF-κB p65/Total NF-κB p65 ratios in both cancer cells. The results of the immunofluorescence and Western blot analyses were validated by the ELISA analysis of p-ERK and p-NF-κB protein levels in MCF-7 (Figure 4F,H) and HepG2 (Figure 4G,I) cells, indicating that phosphorylated Compared to the control and DMSO groups, cancer cells cultured with 30 μM 7-KSS for 24 hours showed a substantial decrease in proteins.

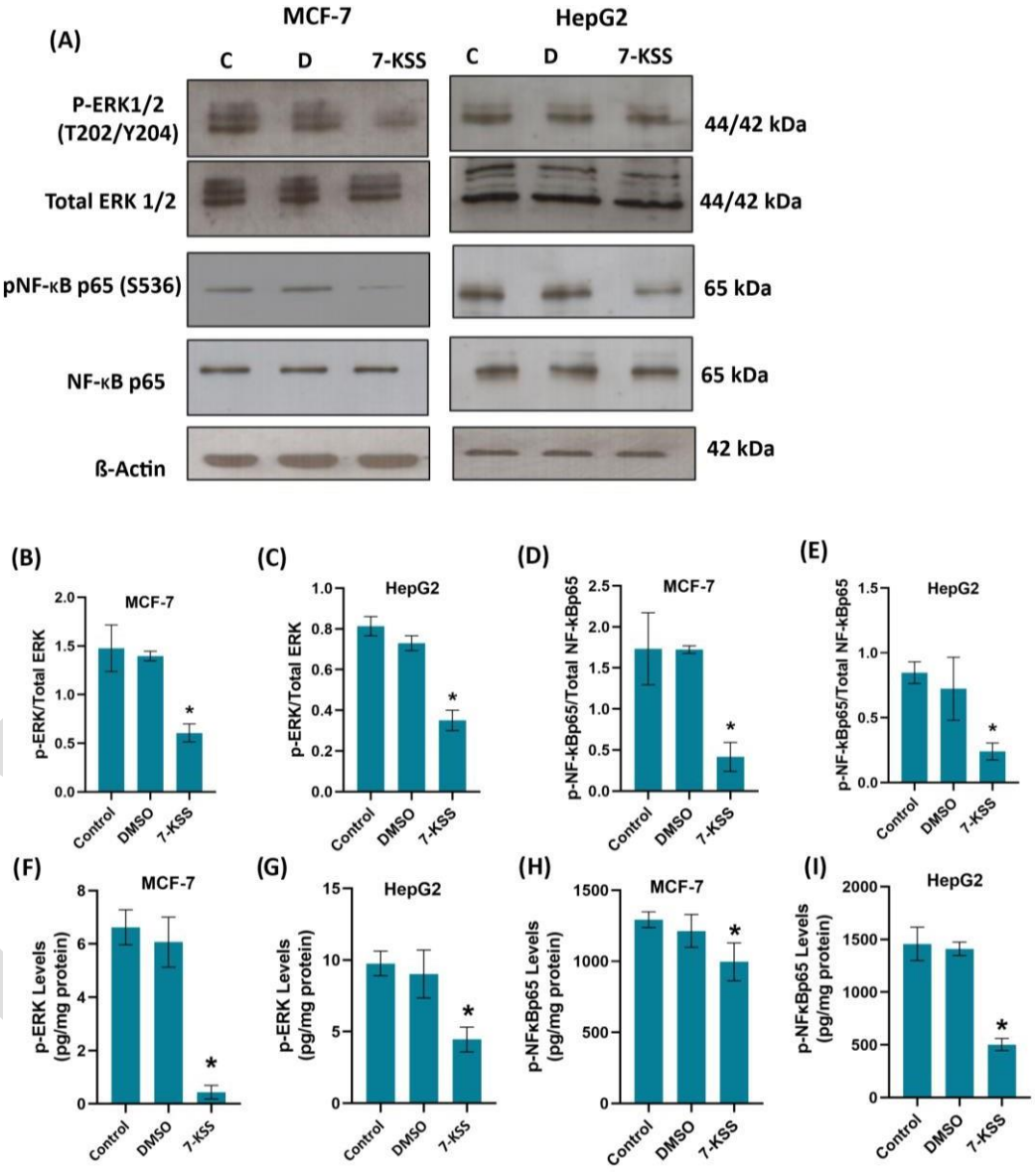

Figure 4. (**A**) Illustrative Western immunoblots for phospho-44/42 ERK1/2 (T202/Y204), total ERK 1/2, phospho-NF-κB p65 (S536), total NF-κB p65, and β-Actin in MCF-7 and HepG2 cells. C, control; D, cells treated with 1 μL/mL dimethyl sulfoxide; 7-KSS, cell treated with 30 μM 7-KSS for 24 h. (**B**) The band quantitation ratio of phospho-ERK/Total ERK in MCF-7 and (**C**) HepG2 cells. (**D**) The band quantitation ratio of phospho-NF-κB p65/Total NF-κB p65 in MCF-7 and (**E**) HepG2 cells. Blots were quantitated by ImageJ software. Data shown are representative of 3 separate experiments and values are given as mean ± SD. Statistical analysis was performed by one-way ANOVA and all pair-wise multiple comparison procedures carried out by the Tukey test. *, $p < 0.01$ vs. control and DMSO groups. (**F**) Phospho-ERK levels in MCF-7 cells. Values mean ± SD ($n = 5–8$). One-way ANOVA and Tukey multiple comparisons were used to determine statistical significance. *, $p < 0.05$ vs. control and DMSO groups. (**G**) Phospho-ERK levels in HepG2 cells. Values mean ± SD ($n = 8$). One-way ANOVA and Tukey multiple comparisons were performed for statistical analysis. *, $p < 0.05$ when compared with the control and DMSO groups. (**H**) Phospho-NF-κB p65 levels in MCF-7 cells. Values mean ± SD ($n = 8$). One-way ANOVA and Tukey multiple comparisons were performed to test statistical significance. *, $p < 0.05$ when compared with the control and DMSO groups. (**I**) Phospho-NF-κB p65 levels in HepG2 cells. Values mean ± SD ($n = 8$). One-way ANOVA and Tukey multiple comparisons were used to determine statistical significance. *, $p < 0.05$ when compared with the control and DMSO groups.

2.5. Apoptosis

A considerable rise in cell death was seen in cancer cells treated with 30 µM 7-KSS for 24 hours according to TUNEL assay (Figure 5A). Apoptotic MCF-7 (Figure 5B) and HepG2 (Figure 5C) cells treated with 7-KSS were significantly more numerous than those in the control and DMSO groups, according to fluorescence labeling for apoptosis quantification. See the illustrative plots of HepG2 and MCF-7 cells in Figure 5D. Within each square, cells that are not yet dead are shown in the lower left corner (annexin V negative/PI negative), cells that are about to die are shown in the upper left corner (annexin V positive), cells that are late in the process of dying are shown in the upper right corner (annexin V positive/PI positive), and cells that have already died are shown in the lower right corner (PI positive). A phospholipid typically located on the inner leaflet of the plasma membrane, annexin V is a protein with a high affinity for PS. During cell death, PS is exposed to the outside world by being translocated from the inner to the outside leaflet of the plasma membrane. One particular target for annexin V binding is PS. The fluorescent dye PI binds to DNA but cannot cross the membranes of living cells. The cell membranes of cells in late stages of apoptosis or necrosis are damaged, thus it may still penetrate these cells. Annexin V and PI staining together make it possible to distinguish between viable cells, cells that have begun to die, cells that have finished dying, and cells that have become necrotic. In Figures 5E and 5F, we can see the flow cytometric quantification of annexin V-FITC labeling in MCF-7 and HepG2 cells, respectively. When compared to the control group, 7-KSS treatment significantly raised the quantity of early and late apoptotic cells.

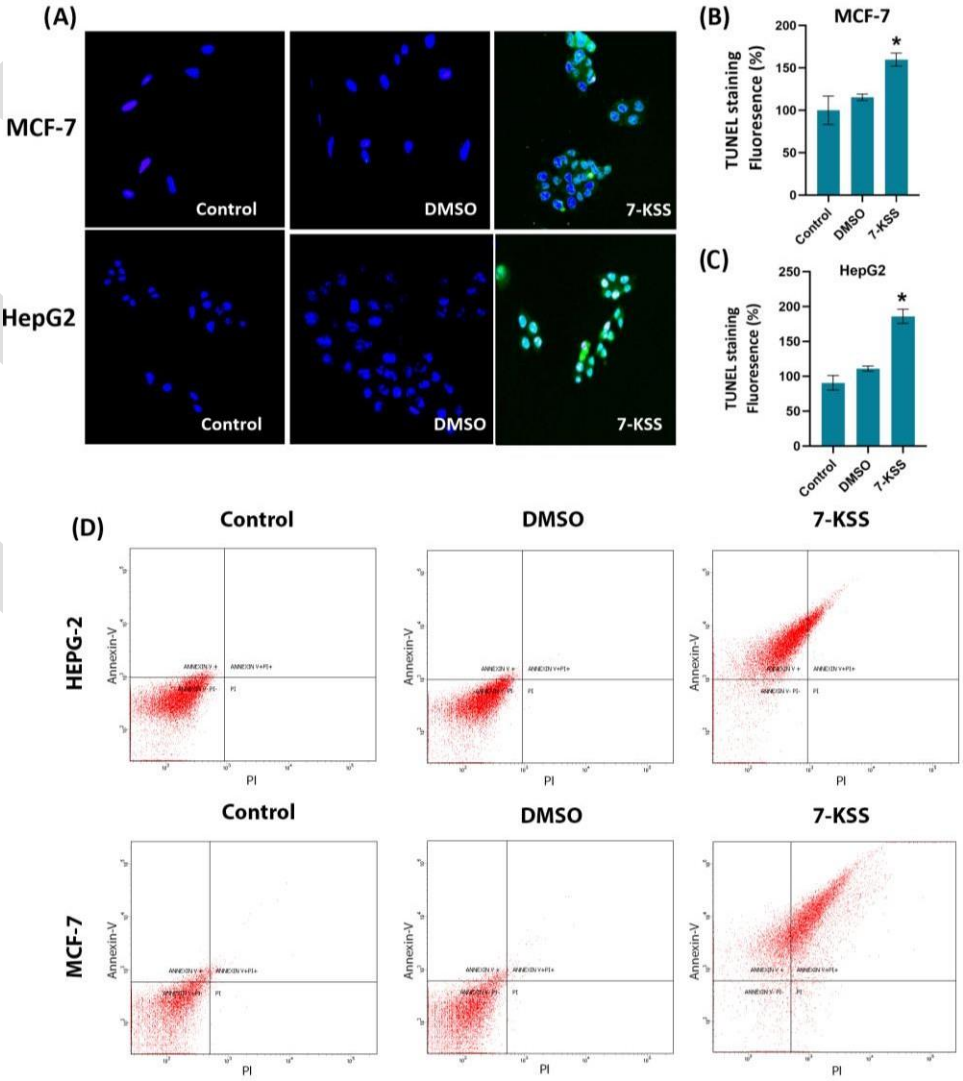

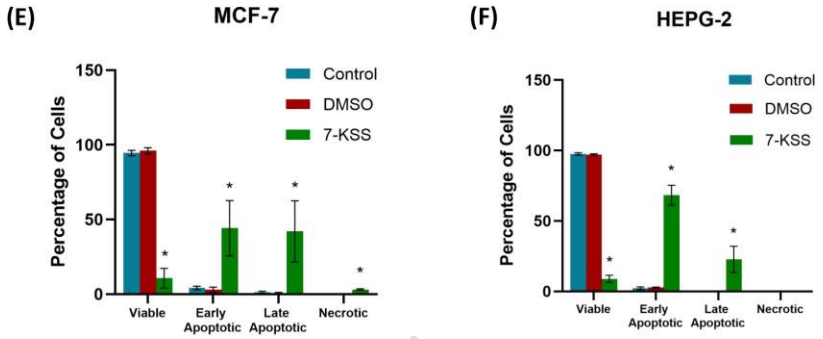

Figure 5. TUNEL staining in cancer cells. (**A**) Dimethyl sulfoxide (DMSO, 1 µL/mL) and 7-KSS (30 µM) were applied for 24 h (200× magnification). (**B**) Quantitation of TUNEL staining in MCF-7 cells with the ImageJ program. Values mean ± SD (n = 7–8). Kruskal–Wallis test and Dunn's analysis were performed to test statistical significance. *, $p < 0.05$ compared with the control and DMSO groups. (**C**) Quantitation of TUNEL staining in HepG2 cells with ImageJ program. Values are mean ± SD (n = 8). One-way ANOVA and Tukey multiple comparisons were used to determine statistical significance. *, $p < 0.05$ when compared with the control and DMSO groups. (**D**) Annexin V–FITC and PI-labeled HepG2 and MCF-7 cells. In total, 10,000 events were analyzed for each condition. (**E**) Quantitative analysis of annexin-V and PI labeling in MCF-7 cells by flow cytometry. Values mean ± SD (n = 3). One-way ANOVA analysis and Tukey test were used for statistical analysis. *, $p < 0.05$ compared to control and DMSO groups. (**F**) Quantitative analysis of annexin-V and PI labeling in HepG2 cells by flow cytometry. Values mean ± SD (n = 3). One-way ANOVA analysis and Tukey test were used for statistical analysis. *, $p < 0.05$ compared to control and DMSO groups.

3. Discussion

The results of this study showed that MCF-7 and HepG2 cancer cells treated with 5-15 µM 7-KSS for 24 hours did not show any significant change in cell viability. After being treated with 30 µM 7-KSS for 24 hours, the viability of cancer cells was significantly decreased. Our finding is consistent with a research that found 30 µM to be the threshold concentration of 7-KSS to achieve subtoxic damage in HepG2 cells at 24 hours [8]. A different research found that after 12 hours of incubation with 120 µM beta-sitosterol oxides, the survival rate of U937 human lung lymphoblastic cells was about 50% lower than the control group, in contrast to the group that did not receive the treatment [26]. Fortunately, even at 30 µM, 7-KSS did not damage noncancerous cells, indicating that it had little cytotoxicity for healthy tissues.

After 24 hours of incubation with cytotoxic doses of 7-KSS, HepG2 and MCF-7 cells showed a significant increase in intracellular levels of C18-C24 ceramides compared to controls. To our knowledge, this is the first investigation into how7-KSS affects the amounts of endogenous sphingolipids in cancer cells of the liver and breast. In line with previous research showing that beta-sitosterol action increased ceramide levels in HT-29 colon cancer cells, our results support this idea [27]. Similarly, a study found that LNCaP human prostate cancer cells treated with 16 µM beta-sitosterol experienced apoptosis and a significant uptick in ceramide synthesis [28]. Additionally, the effects of dietary β-sitosterol on the proliferation and ceramide concentrations of MCF-7 and MDA-MB-231 human breast cancer cells were investigated. The results demonstrated that beta-sitosterol increased serine palmitoyl transferase activity, which in turn stimulated de novo ceramide production [29]. Additionally, we found that cancer cell S1P levels were significantly decreased after 24 hours of treatment with 30 µM 7-KSS. Our research indicates that 7-KSS treatment of cancer cells results in decreased S1P levels, which is the first of its kind. Ceramide and S1P are functional sphingolipid metabolites that play an essential role in the activity of many pathways that are fundamental to the development of cancer. Modern understanding of physiologically active sphingolipid production acknowledges its critical functions in the initiation and progression of cancer. Ceramide inhibits tumor growth by activating anti-proliferative mechanisms; it is an essential chemical in sphingolipid metabolism.

and death processes in a large number of malignant cells [30]. Instead, S1P is a lipid that promotes cancer due to the processes it triggers.

The mechanism by which 7-KSS enhances ceramide production in HepG2 and MCF-7 cells remains unexplained by our results. Phytosterols, which have a structure different from cholesterol, may interact with enzymes in the ceramide production pathway in a manner that alters the fluidity of the cell membrane. A previous research found that rats given a diet containing 2% cholesterol and 3% β-sitosterol for 21 days had less fluidity in their liver membranes [31]. Some degrees of membrane fluidity may be required for the optimal functioning of enzymes attached to membranes [32]. A byproduct of beta-oxidation sitosterol, 7-KSS, may upregulate enzymes involved in ceramide production, including ceramide synthase (CerS) and serine palmitoyltransferase (SPT) [29,33], much like beta-sitosterol itself. Ceramide levels may be increased by 7-KSS, similar to campesterol, by downregulating ceramidases [34]. Ceramidases break down ceramides into sphingosine and fatty acids.

In cancer cells treated with 7-KSS, compared to the control groups, we observed a substantial suppression of phosphorylated 44/42 ERK1/2 and phosphorylated NF-κB p65 (Ser536) proteins. Our understanding is that this is the first work to document that 7-KSS suppresses ERK1/2 and NF-κB phosphorylation in cancer cells. While few biological phytosterol oximes have been studied, one that did reduce cell viability in MCF-7 cells via apoptosis and down regulation of the ERK1/2 signaling pathway was 7-alpha-OH-beta-sitosterol [35]. There were no obvious effects on ERK1/2 expression when the phytosterol fucosterol, which is obtained from marine algae and several plant types, was discovered to decrease phosphorylated ERK1/2 expression [36]. Integral to the MAPK signaling cascade are phospho-44/42 ERK1/2, or phosphorylated extracellular signal-regulated kinases 1 and 2 [37]. One possible therapeutic target for cancer is ERK1/2, as its aberrant phosphorylation is associated with tumor etiology [37]. Multiple biological activities, such as cell proliferation, differentiation, survival, and apoptosis, are fundamentally regulated by this route. There is a strong correlation between cell proliferation and growth and ERK1/2 phosphorylation [38]. There is evidence that phosphorylated ERK1/2 signaling plays a role in cell differentiation as well [38]. By preventing cancer cells from undergoing cell death, ERK1/2 phosphoryla-tion may enhance cell survival [39]. A possible mechanism by which 7-ketositosterol inhibits ERK signaling is by increasing the activity of MAPK phosphatases, which in turn deactivate ERKs, or by blocking upstream activators such as Ras. Similar to beta-sitosterol, 7-KSS may hinder ERK activation via interactions with membrane receptors or signaling molecules [42].

The anticancer effects of several phytosterols have been documented, and they work by reducing inflammatory cytokines and chemokines that target NF-κB signaling and by blocking NF-κB activation [20]. The transcription factor NF-κB p65 has two activation domains called TA1 and TA2, as well as signals for nuclear localization and areas for binding to DNA. An essential trans-activation domain, the TA1 region has 30 amino acids at its C-terminus. Several phosphorylation processes occurring within this region are necessary for NF-κB transactivation. Ser536 inside TA1 is one of these critical phosphorylation sites that is conserved across different species. Its transcriptional activity is increased by phosphorylating p65. The number 43. In pancreatic cancer cells, beta-sitosterol was shown to reduce levels of phospho-NF-κB p65 but had no effect on overall NF-κB p65 levels [44]. It is possible that 7-keto-sitosterol reduces the transcription of pro-inflammatory genes by blocking the phosphorylation and degradation of IκBα, an inhibitor of NF-κB, which in turn inhibits the activation of NF-κB [45]. The activation of NF-κB might be reduced if 7-ketositosterol directly interacts with components of the NF-κB signaling pathway, for as by inhibiting the activity of IκB kinase (IKK) [45].

As previously mentioned, phytosterols' anticancer effects are due in large part to their ability to induce apoptosis and stimulate ceramide production. Analysis using TUNEL, as

annexin V-FITC/PI staining and other methods demonstrated that cancer cells exposed to 30 μM

7-KSS for 24 hours exhibited a significant upregulation of cell death. In humans, 7-KSS has been shown to enhance early apoptosis in HepG2 cells [14], U937 cells (a type of leukemia), and intestinal cancer cells [46, 47]. Our results corroborate these prior findings.
It is critical to acknowledge the limits of cancer cell culture research, despite the fact that these investigations may substantially help fundamental biological processes and early drug testing. To get a more comprehensive grasp of cancer biology and treatment responses, these research should include in vivo models and clinical data. Contrary to what is seen in live animals, the intricate tumor microenvironment of cultured cancer cells does not contain stromal cells, immune cells, the extracellular matrix, or blood vessels. Traditional two-dimensional cell cultures can't capture the complex three-dimensional structure of tumors, which might influence how drugs interact with cells and how they behave. Due to genetic and phenotypic changes that occur throughout time, cancer cell lines might vary from the initial tumor and from subculture to subculture. The original tumor's heterogeneity may not be accurately reflected in the selection forces that result from continuous passage and adaption to in vitro circumstances. These pressures favor the survival of particular cell populations. There may be differences in medication reactions and cellular metabolism between the tumor microenvironment and cell culture media due to differences in nutritional makeup and oxygen concentrations. Absorption, distribution, metabolism, and excretion of drugs in living beings cannot be accurately predicted by the pharmacokinetics and pharmacodynamics of drug administration in cell cultures. The heterogeneity inside tumors that might impact treatment results is overlooked in many cancer cell culture research because they only concentrate on one kind of cancer cell.
To summarize, adding 7-KSS to cancer cells led to a decrease in cell viability, suppression of proliferating cell nuclear antigen, S1P, p-ERK, and p-NF-κB p65 protein levels, and an increase in ceramide quantities and apoptotic cell counts. Reduced proliferation in cancer cells treated with 7-KSS, which may facilitate apoptosis, is caused by increased ceramide concentrations, decreased S1P, decreased phospho-44/42 ERK1/2, and dropped phospho-NF-κB p65 levels. Our research indicates that 7-KSS has promise as a cancer treatment agent, mainly due to its capacity to trigger cell death and alter important signaling pathways. Applying these in vitro findings in a clinical setting should be the focus of future study. We hope that future research using animal models of cancer will confirm our in vitro results. The safety and efficacy of 7-KSS in a more complex biological system should be better understood with the aid of these investigations. Outlining the pathways involved in 7-KSS-induced apoptosis and the rise in ceramide levels might be achieved via the use of particular inhibitors or transgenic models. It would be interesting to see how 7-KSS treatment plays out when combined with other targeted treatments or chemotherapeutic medicines to see if there are any synergistic effects that might boost the effectiveness of the treatment. For a more realistic simulation of the clinical setting and validation of the results, patient-derived cancer cells and organoids might be used. Better and more personalized cancer treatments may be in the future if these questions are answered, which might improve our knowledge of 7-KSS's action mechanisms and its possible function in cancer therapy.

4. Materials and Methods

4.1. Cell Culture

The cell lines used in this study were sourced from the American Type Culture Collection (ATCC) in Manassas, VA, USA. The human breast cancer (MCF-7) and liver cancer (HepG2) cell lines were also used. The cells known as MCF-7 were grown in a culture medium called Dulbecco's Modified Eagle's Medium (DMEM)-F12. This medium was supplied by Biowest and was sourced from Nuaillé, France. It also contained 10% (v/v) heat-inactivated fetal bovine serum (FBS) from Gibco, Life Technologies, Grand Island, NY, USA, 100 U/mL penicillin, 100 µg/mL streptomycin, 5 µg/100 mL amphotericin B, and 2.5 mM L-Glutamine, which were all from Gibco. 3.7 g/L of sodium bicarbonate was added to the DMEM high-glucose medium (Sigma; Cat.#D5648, St. Louis, MO, USA) when HepG2 and BJ cells were cultivated.
(Gibco), 5 µg/100 mL amphotericin B, 10% (v/v) FBS, 100 U/mL penicillin, 100 µg/mL streptomycin, and 1% sodium pyruvate (Sigma-Aldrich). In a controlled environment of 37°C, 5% CO2, and 95% humidity, the cells were cultured in an incubator. When the cell density reached 80% confluency, the cells were transferred to fresh flasks by removing them from the surface and suspending them in a solution of trypsin-EDTA (0.05% Tryp-sin/0.02% EDTA; Gibco).

Treatment with 7-ketositosterol (4.2) Commercially available 7-KSS (MW = 428.7 g/mol; Cayman, Cat.#37189, Ann Arbor, MI, USA) was used in our investigation. To create an 11.66 mM stock solution, 5 mg of 7-KSS was diluted in 1 mL of DMSO. Using cell culture medium, a 1 mM intermediate stock was prepared. The MTT [3-(4,5- dimethylthiazol-2-yl)-2,5-diphenyltetrazolium bromide] study used 7, 10, 15, and 30 μM 7-KSS as its final concentrations. The final dosage and duration of 7-KSS administration in MCF-7 and HepG2 cells were determined using data from MTT analyses4.3. Analysis of MTT The following cell types were introduced into 96-well plates: MCF-7, HepG2, and BJ. After being left to adhere overnight, the cells were treated with culture media that contained either 1 μL/mL DMSO or 5-30 μM 7-KSS. After12,18, and 24 hours of incubation, the MTT procedure was initiated. A 0.22 μm pore filter was used to filter out MTT after dissolving it in PBS (5 mg/mL) from Gold Biotechnology Inc. in St. Louis, MO, USA. After removing the incubation media, 90 μL of fresh medium and 10 μL of MTT were added to each well by volume. Purple formazan crystals were produced after 2 hours of incubation with MTT at 37 °C, and 100 μL of DMSO was then added. Two wavelengths, 570 and 690 nm, were used in a spectrophotometric plate reader to quantify absorbance. The cell viability percentage was determined by dividing the absorbance of the control group by that of the sample, and then multiplying the result by 100. For every cell line, three distinct experimental groups were established: control, DMSO (1 μL/mL), and 7-KSS (MCF-7 and HepG2 cells treated with 30 μM 7-KSS for 24 hours). Four Chapters on Immunofluorescent Staining
We used chamber slides from Merck Millipore in Cork, Ireland, with 100,000 cells per well, to transfer MCF-7 and HepG2 cells. To ensure cell adhesion, the chamber slides were incubated overnight at 37 °C in a 5% CO2 incubator. After 24 hours of incubation, the treatment media was added to the culture medium after the cells achieved 70% confluency. Two washes with 0.01 M cold PBS were performed on the removed medium. The cells were left to fix at room temperature for 10 minutes after 250 μL of newly made 4% paraformaldehyde was added. The cells were washed twice with PBS buffer after the fixing solution was aspirated. To initiate the permeabilization process, 300 μL of PBS containing 0.2% Triton X-100 (Sigma-Aldrich, St. Louis, MO, USA) was mixed, then incubated at room temperature for 30 minutes. Prior to blocking with 5% normal goat serum (NGS; Vector Laboratories, Burlingame, CA, USA), cells were washed five times with cold PBS. After the blocking solution was removed, cells were exposed to phospho-p44/42 ERK1/2 (1:200 dilution, Cat.#9101, Cell Signaling Tech., Massachusetts, USA), phospho-NF-κB p65 (1:200 dilution, Cat.#AF2006, Affinity Biosciences, Changzhou, Jiangsu, China), and PCNA (1:200 dilution, Cat.#bs-0754R, Bioss Antibodies Inc., Woburn, MA, USA) antibodies at 200 μL per well for an overnight period at 4 °C without washing. The next day, under dark conditions, the chamber slides were washed five times with PBS at room temperature before being incubated for 45 minutes with 200 μL of Alexa Fluor-488 conjugated goat anti-rabbit (1:1000, Cat.#ab150077 Abcam, Cambridge, UK) secondary antibody. Once the chamber slide assembly had been washed three times with PBS, a drop of DAPI (Vector Laboratories Inc., Burlingame, CA, USA) was carefully poured onto the slide to stain the nucleus. The slide was then covered with a bubble-free coverslip. The fluorescent microscope (Olym-pus IX81, Tokyo, Japan) was used at a magnification of 20× to examine the slides. The 488 nm excitation was used to photograph the Alexa Flour. The excitation and emission wavelengths for DAPI were 350 nm and 440-460 nm, respectively, whereas those for other samples were 505-525 nm. We used NIH ImageJ 1.53e software to measure the fluorescence intensity in HepG2 and MCF-7 cells. The total cell fluorescence (CTCF) that was validated for each individual cell in each group was calculated using the following formula: CTCF = Integrated Density − (Area of the chosen cell × Background mean fluorescence).

4.5. Elispot Assay Enzyme-Linked An ELK Biotechnology non-competitive sandwich ELISA kit (Cat.#ELK5141) was used to assess proliferating cell nuclear antigen (PCNA) in Denver, CO, USA. The research groups determined the dosage of MCF-7 and HepG2 cells, which were then suspended in PBS at a concentration of 107 cells/mL. The cells were then ultrasonicated and centrifuged at 2-8 °C for 10 minutes at 1500× g. We followed the manufacturer's instructions to conduct PCNA measurements in supernatants. Using a PCNA standard curve, the concentration of PCNA in the samples was measured at 450 nm and expressed as nanograms per milligram of protein. An ELK Biotechnology non-competitive sandwich ELISA kit (Cat.#ELK8541; Denver, CO, USA) was used for phospho-ERK studies. The MCF-7 and HepG2 cells were divided into different groups based on their dosage. After collecting the cells (107 cells/mL), they were mixed with PBS and put through ultrasonication. After that, they were centrifuged at 2-8 °C for 10 minutes at 1500× g. Upon the manufacturer's instruction, phospho-ERK assays were carried out in the supernatants. The samples' p-ERK concentration was measured at 450 nm using a p-ERK standard curve. The results were presented as pg/mg protein. Non-competitive sandwich ELISA kits (BT Lab, Bioassay

Technology Laboratory; Shanghai, China, Cat.#E4753Hu) were used to quantify phospho-NF-κB p65 (ser536) in accordance with the instructions provided by the manufacturer. The groups of research determined the dosage of MCF-7 and HepG2 cells, which were then resuspended in PBS at a concentration of 106 cells/mL. The cells were then ultrasonicated and centrifuged at 2-8 °C for 20 minutes at 1500 × g. Protein concentration of p-NF-κB p65 (ser536) was measured in the samples at 450 nm using a standard curve and given as pg/mg. Western blot analysis (4.6) Following the procedures outlined in [48], Western blot analysis was carried out. Before combining the cell lysates from the different treatment groups, 2-mercaptoethanol was added to the Laemmli sample buffer (Cat.# 161-0737, BioRad Laboratories Inc., Hercules, CA, USA). The 30 µL sample, which contained 30 µg of protein, was separated using 12% Mini-protean TGX precast electrophoresis gels (Cat.#4561043, BioRad Laboratories Inc., USA) after the proteins were denaturated at 100 +/-°C. After immobilizing proteins on nitrocellulose membranes using a Trans-Blot SD Semi-Dry Transfer Cell (BioRad Laboratories Inc., USA), the membranes were rinsed with 10 mL of blocking solution (2% bovine serum albumin (BSA) in PBS) and left to sit at room temperature for 5 minutes. After dilution in blocking solution, the primary antibodies were applied and left at room temperature for 1 hour. The primary antibodies used in the experiment were phospho-44/42 ERK1/2 (1:1000 dilution, Cat.#9101, Cell Signaling Tech., Danvers, MA, USA), phospho-NF-κB p65 (Ser536) (1:500 dilution, Cat.#AF2006, Affinity Biosciences, Jiangsu, China), NF-κB p65 (1:2000 dilution, Cat.#ab16502, Abcam Limited, Cambridge, UK), ERK1/2 (1:2000 dilution, Cat.#AF0155, Affinity Biosciences, Changzhou, Jiangsu, China), and beta Actin (1:1000 dilu-tion, Cat.#ab8227, Abcam Limited, Cambridge, UK). In a total of five washes, the blots were immersed in 10 mL of Tris Buffered Saline (TBS) containing 0.05% Tween 20 for 5 minutes each. The blots were washed five times in 10 mL of TBS containing 0.05% Tween 20 after being incubated with the secondary antibody, Goat Anti-Rabbit IgG HRP-conjugate (1:10,000 dilution, Cat.# 632131, Sigma-Aldrich, St. Louis, MO, USA), for one hour at room temperature. It was the Amersham Pharmacia Biotech ECL reagent in Buckinghamshire, UK, that was used to see the immunoreactive bands. The NIH ImageJ 1.53e program was used for image processing and quantification of all Western blots. 4.7. Apoptotic Cell Count Determination Apoptotic cells were detected using the One-Step TUNEL Test Kit (Elabscience, Cat#E-CK-A320, Houston, TX, USA). When DNA is broken, the exposed 3′-OH ends may be used to add fluorescein-labeled dUTP by means of Terminal Deoxynucleotidyl Transferase (TdT). Following the instructions on the test kit, we prepared the reagents and samples. At a density of around 100,000 cells/well, MCF-7 and HepG2 cells were transplanted onto chamber slides. After 24 hours of incubation, the treatment media was added to the culture medium after the cells achieved 70% confluency. The positive control group underwent DNA cleavage with DNase I to disclose 3′-OH ends. After adding 100 µL of DNase I solution (200 U/mL), the cells were left to incubate at 37 °C for 20 minutes. We used PBS to wash the slides three times, each time for five minutes. The cells used as negative controls were incubated with DNase I buffer for 5 minutes at room temperature before being rinsed three times with PBS for 5 minutes each. The addition of 100 µL of TdT balancing buffer was made after the experimental groups finished the penetration stage, and the slides were then incubated at 37 °C for 25 minutes. After the time was up, 50 µL of labeling solution was applied to every slide and left to incubate in a humidified atmosphere at 37 °C for 60 minutes. None of the working solutions used for negative control labeling included TdT enzyme. The incubation period came to a close with three 5-minute washes of the slides in PBS. One drop of DAPI was dropped over the slides after the chambers were separated and cleaned with a napkin. A clean coverslip, free of air bubbles, was then sealed. Next, the fluorescence intensity of the slides was examined using Image J software (NIH) after being seen using a fully automated Olympus BX61 microscope. The apoptotic effects of 7-KSS on breast cancer cells and liver cancer cells were also assessed using a PI apoptosis kit and FITC-conjugated annexin-V (#E-CK-A211, Elabscience, Houston, TX, USA). Cell groups were formed according to the methods outlined before. We threw out the media after each application. Trypsinization was used to remove the cells from the surface of the flask after washing. After centrifugation at 125× g for 5 minutes at +4 °C, the supernatant was removed in order to extract the cells from the solution that contained trypsin. A total of 1 x 10^1 cells were moved to the flow cytometry tube after being suspended in PBS. The supernatant was collected after 5 minutes of centrifugation at 125× g. The annexin-V binding buffer was added to 500 µL of cell suspension. Five microliters of PI reagents and five microliters of FITC-labeled annexin-V were combined and incubated with the cells for twenty minutes at room temperature. Flow cytometry was used to rapidly examine fluorescently conjugated cells after incubation using the correct parameters (FACS Canto II, BD Bioscience, San Jose, CA, USA). Analysis was conducted using BD FACS Diva 6.1.3 software from BD Bio-sciences.

Measurements of Sphingolipids by Mass Spectrometry (4.8)
The HepG2 and MCF-7 cell lysates, which contain 10 mg protein/mL, were produced by mixing 2

μL of an IS stock solution with 5 μg/mL. Once the tubes had been vortexed, 100 μL of distilled water was added, followed by sonication for 30 seconds and vortexing for 5 minutes. Then, a mixture of 1:2 chloroform: methanol by volume was added. After 30 minutes of incubation at room temperature, the mixture was spun at 2000× g for 5 minutes to extract the supernatants. The supernatants were mixed with 125 μL of chloroform and 125 μL of distilled water, then vortexed and left at room temperature for 30 minutes with no further action. Following the incubation period, around 500 μL of the top-organic layer was moved to a fresh glass tube and subjected to a continuous nitrogen flow to initiate the volatilization process. The samples were prepared for LC-MS/MS measurements by dissolving the dried residues in a solution of methanol and formic acid (100 μL; 99.9:0.1). Then, the samples were transferred to insert vials. The LC-MS/MS analyses followed the procedures detailed elsewhere [49]. Section 4.9: Protein Assays
A modified Bradford assay was used to quantify protein concentrations at 595 nm. Thermo Fisher Scientific Cat.# 23238, Waltham, MA, USA, was supplied by Thermo Fisher, and bovine serum albumin served as the standard. 4.10. Analyzing Statistics
We used GraphPad Prism 9.00 and SigmaPlot 15 for Windows (Systat Software, Inc., St. Palo Alto, CA, USA) to analyze the data. A statistically significant result was defined as a p value less than 0.05. The statistical analysis for each measurement is described in depth in the figure and table legends. Before the groups were compared using statistical analysis, a normalcy test was conducted. We used a nonparametric test when the data did not follow a normal distribution.

Funding: This work was supported by grants from Akdeniz University Research Foundation BAP-SIS (grant number: TSA-2023-6282).

Data Availability Statement: Data obtained and analyzed in this work are available from the corresponding author on reasonable request.

Conflicts of Interest: The authors declare no conflicts of interest.

Abbreviations

7-KSS: 7-ketositosterol; AP1, activated protein 1; CERs, ceramides; CTCF, validated total cell fluorescence; ERKs, extracellular signal-regulated kinases; MAPKs, mitogen-activated protein kinases; NF-κB, nuclear factor kappa B; PCNA, proliferating cell nuclear antigen; PI, propidium iodide; POPs, phytosterol oxidation products; S1P, sphingosine-1-phosphate; SMs, sphingomyelins; TLR4, toll-like receptor 4; UV, ultraviolet.

References

1. Jefrei, E.; Xu, M.; Moore, J.B.; Thorne, J.L. Phytosterol and phytostanol-mediated epigenetic changes in cancer and other non-communicable diseases: A systematic review. *Br. J. Nutr.* **2024**, *131*, 935–943. https://doi.org/10.1017/s0007114523002532. PMID: 37955052; PMCID: PMC10876456.
2. Ramprasath, V.R.; Awad, A.B. Role of Phytosterols in Cancer Prevention and Treatment. *J. AOAC Int.* **2015**, *98*, 735–738. https://doi.org/10.5740/jaoacint.sgeramprasath. PMID: 26086253.
3. Plat, J.; Brzezinka, H.; Lütjohann, D.; Mensink, R.P.; von Bergmann, K. Oxidized plant sterols in human serum and lipid infusions asmeasured by combined gas-liquid chromatography-mass spectrometry. *J. Lipid Res.* **2001**, *42*, 2030–2038. PMID: 11734576.
4. El Omari, N.; Bakrim, S.; Khalid, A.; Abdalla, A.N.; Iesa, M.A.M.; El Kadri, K.; Tang, S.Y.; Goh, B.H.; Bouyahya, A. Unveiling the molecular mechanisms: Dietary phytosterols as guardians against cardiovascular diseases. *Nat. Prod. Bioprospect.* **2024**, *14*, 27. https://doi.org/10.1007/s13659-024-00451-1. PMID: 38722432; PMCID: PMC11082103.
5. Khan, Z.; Nath, N.; Rauf, A.; Bin Emran, T.; Mitra, S.; Islam, F.; Chandran, D.; Barua, J.; Khandaker, M.U.; Idris, A.M.; et al. Multifunctional roles and pharmacological potential of β-sitosterol: Emerging evidence toward clinical applications. *Chem. Interact.* **2022**, *365*, 110117. https://doi.org/10.1016/j.cbi.2022.110117. PMID: 35995256.
6. Salehi, B.; Quispe, C.; Sharifi-Rad, J.; Cruz-Martins, N.; Nigam, M.; Mishra, A.P.; Konovalov, D.A.; Orobinskaya, V.; Abu-Reidah, I.M.; Zam, W.; et al. Phytosterols: From Preclinical Evidence to Potential Clinical Applications. *Front. Pharmacol.* **2021**, *11*, 599959. https://doi.org/10.3389/fphar.2020.599959. PMID: 33519459; PMCID: PMC7841260.
7. Poli, A.; Marangoni, F.; Corsini, A.; Manzato, E.; Marrocco, W.; Martini, D.; Medea, G.; Visioli, F. Phytosterols, Cholesterol Control, and Cardiovascular Disease. *Nutrients* **2021**, *13*, 2810. https://doi.org/10.3390/nu13082810. PMID: 34444970; PMCID: PMC8399210.
8. Woyengo, T.A.; Ramprasath, V.R.; Jones, P.J.H. Anticancer effects of phytosterols. *Eur. J. Clin. Nutr.* **2009**, *63*, 813–820. https://doi.org/10.1038/ejcn.2009.29. PMID: 19491917.

9. Wang, H.; Wang, Z.; Zhang, Z.; Liu, J.; Hong, L. β-Sitosterol as a Promising Anticancer Agent for Chemoprevention and Chemotherapy: Mechanisms of Action and Future Prospects. *Adv. Nutr. Int. Rev. J.* **2023**, *14*, 1085–1110. https://doi.org/10.1016/j.advnut.2023.05.013. PMID: 37247842; PMCID: PMC10509430.
10. Nandi, S.; Nag, A.; Khatua, S.; Sen, S.; Chakraborty, N.; Naskar, A.; Acharya, K.; Calina, D.; Sharifi-Rad, J. Anticancer activity and other biomedical properties of β-sitosterol: Bridging phytochemistry and current pharmacological evidence for future translational approaches. *Phytother. Res.* **2024**, *38*, 592–619. https://doi.org/10.1002/ptr.8061. PMID: 37929761.
11. García-Llatas, G.; Rodríguez-Estrada, M.T. Current and new insights on phytosterol oxides in plant sterol-enriched food. *Chem. Phys. Lipids* **2011**, *164*, 607–624. https://doi.org/10.1016/j.chemphyslip.2011.06.005. PMID: 21699886.
12. Liu, J.; Wang, D.; Shao, P.; Feng, S. Photooxidation stability of phytosterols with different relative spatial positions in different particles. *Food Innov. Adv.* **2023**, *2*, 225–232. https://doi.org/10.48130/fia-2023-0024.
13. Scholz, B.; Guth, S.; Engel, K.; Steinberg, P. Phytosterol oxidation products in enriched foods: Occurrence, exposure, and biological effects. *Mol. Nutr. Food Res.* **2015**, *59*, 1339–1352. https://doi.org/10.1002/mnfr.201400922. PMID: 25787244.
14. Koschutnig, K.; Heikkinen, S.; Kemmo, S.; Lampi, A.-M.; Piironen, V.; Wagner, K.-H. Cytotoxic and apoptotic effects of single and mixed oxides of beta-sitosterol on HepG2-cells. *Toxicol. In Vitro* **2009**, *23*, 755–762. https://doi.org/10.1016/j.tiv.2009.03.007. PMID: 19328846.
15. Kenny, O.; O'callaghan, Y.; O'connell, N.M.; McCarthy, F.O.; Maguire, A.R.; O'brien, N.M. Oxidized derivatives of dihydrobrassicasterol: Cytotoxic and apoptotic potential in U937 and HepG2 Cells. *J. Agric. Food Chem.* **2012**, *60*, 5952–5961. https://doi.org/10.1021/jf204737e. PMID: 22594485.
16. Conchillo, A.; Cercaci, L.; Ansorena, D.; Rodriguez-Estrada, M.T.; Lercker, G.; Astiasarán, I. Levels of phytosterol oxides in enriched and nonenriched spreads: Application of a thin-layer chromatography–gas chromatography methodology. *J. Agric. Food Chem.* **2005**, *53*, 7844–7850. https://doi.org/10.1021/jf050539m. PMID: 16190640.
17. Bradford, P.G.; Awad, A.B. Modulation of signal transduction in cancer cells by phytosterols. *BioFactors* **2010**, *36*, 241–247. https://doi.org/10.1002/biof.97. PMID: 20818709.
18. Shi, M.; Tang, C.; Wu, J.-X.; Ji, B.-W.; Gong, B.-M.; Wu, X.-H.; Wang, X. Mass Spectrometry Detects Sphingolipid Metabolites for Discovery of New Strategy for Cancer Therapy from the Aspect of Programmed Cell Death. *Metabolites* **2023**, *13*, 867. https://doi.org/10.3390/metabo13070867. PMID: 37512574; PMCID: PMC10384871.
19. Guo, Y.J.; Pan, W.W.; Liu, S.B.; Shen, Z.F.; Xu, Y.; Hu, L.L. ERK/MAPK signalling pathway and tumorigenesis. *Exp. Ther. Med.* **2020**, *19*, 1997–2007. https://doi.org/10.3892/etm.2020.8454. PMID: 32104259; PMCID: PMC7027163.
20. Khan, A.U.; Khan, A.; Shal, B.; Khan, S.; Khan, M.; Ahmad, R.; Riaz, M. The critical role of the phytosterols in modulating tumor microenvironment via multiple signaling: A comprehensive molecular approach. *Phytother. Res.* **2023**, *37*, 1606–1623. https://doi.org/10.1002/ptr.7755. PMID: 36757068.
21. Jarvis, W.D.; Fornari, F.A.; Auer, K.L.; Freemerman, A.J.; Szabo, E.; Birrer, M.J.; Johnson, C.R.; Barbour, S.E.; Dent, P.; Grant, S. Coordinate regulation of stress- and mitogen-activated protein kinases in the apoptotic actions of ceramide and sphingosine. **1997**, *52*, 935–947. https://doi.org/10.1124/mol.52.6.935. PMID: 9415703.
22. Roy, A.; Srivastava, M.; Saqib, U.; Liu, D.; Faisal, S.M.; Sugathan, S.; Bishnoi, S.; Baig, M.S. Potential therapeutic targets for inflammation in toll-like receptor 4 (TLR4)-mediated signaling pathways. *Int. Immunopharmacol.* **2016**, *40*, 79–89. https://doi.org/10.1016/j.intimp.2016.08.026. PMID: 27584057.
23. Aggarwal, B.B. Nuclear factor-κB. *Cancer Cell* **2004**, *6*, 203–208. https://doi.org/10.1016/j.ccr.2004.09.003. PMID: 15380510.
24. Eskiler, G.G.; Özkan, A.D.; Kaleli, S.; Bilir, C. Inhibition of TLR4/TRIF/IRF3 Signaling Pathway by Curcumin in Breast Cancer Cells. *J. Pharm. Pharm. Sci.* **2019**, *22*, 281–291. https://doi.org/10.18433/jpps30493. PMID: 31287789.
25. Hsiao, C.-C.; Chen, P.-H.; Cheng, C.-I.; Tsai, M.-S.; Chang, C.-Y.; Lu, S.-C.; Hsieh, M.-C.; Lin, Y.-C.; Lee, P.-H.; Kao, Y.-H. Toll-like receptor-4 is a target for suppression of proliferation and chemoresistance in HepG2 hepatoblastoma cells. *Cancer Lett.* **2015**, *368*, 144–152. https://doi.org/10.1016/j.canlet.2015.08.004. PMID: 26276725.
26. Maguire, L.; Konoplyannikov, M.; Ford, A.; Maguire, A.R.; O'Brien, N.M. Comparison of the cytotoxic effects of beta-sitosterol oxides and a cholesterol oxide, 7beta-hydroxycholesterol, in cultured mammalian cells. *Br. J. Nutr.* **2003**, *90*, 767–775. https://doi.org/10.1079/bjn2003956. PMID: 13129445.
27. Awad, A.B.; Von Holtz, R.L.; Cone, J.P.; Fink, C.S.; Chen, Y.C. beta-Sitosterol inhibits growth of HT-29 human colon cancer cells by activating the sphingomyelin cycle. *Anticancer. Res.* **1998**, *18*, 471–473; Erratum in: *Anticancer Res.* **1998**, *18*, 1227. PMID: 9568122.
28. von Holtz, R.L.; Fink, C.S.; Awad, A.B. beta-Sitosterol activates the sphingomyelin cycle and induces apoptosis in LNCaP human prostate cancer cells. *Nutr. Cancer* **1998**, *32*, 8–12. https://doi.org/10.1080/01635589809514709. PMID: 9824850.
29. Awad, A.B.; Barta, S.L.; Fink, C.S.; Bradford, P.G. beta-Sitosterol enhances tamoxifen effectiveness on breast cancer cells by affecting ceramide metabolism. *Mol. Nutr. Food Res.* **2008**, *52*, 419–426. https://doi.org/10.1002/mnfr.200700222. PMID: 18338406.
30. Ogretmen, B. Sphingolipid metabolism in cancer signalling and therapy. *Nat. Rev. Cancer* **2018**, *18*, 33–50. https://doi.org/10.1038/nrc.2017.96. PMID: 29147025; PMCID: PMC5818153.
31. Leikin, A.I.; Brenner, R.R. Fatty acid desaturase activities are modulated by phytosterol incorporation in microsomes. *Biochim. Biophys. Acta BBA Lipids Lipid Metab.* **1989**, *1005*, 187–191. https://doi.org/10.1016/0005-2760(89)90186-0. PMID: 2775772.
32. Pande, A.H.; Qin, S.; Tatulian, S.A. Membrane fluidity is a key modulator of membrane binding, insertion, and activity of 5-lipoxygenase. *Biophys. J.* **2005**, *88*, 4084–4094. https://doi.org/10.1529/biophysj.104.056788. PMID: 15778441; PMCID: PMC1305639.

33. Takeda, S.; Terazawa, S.; Shimoda, H.; Imokawa, G. β-Sitosterol 3-*O*-D-glucoside increases ceramide levels in the stratum corneum via the up-regulated expression of ceramide synthase-3 and glucosylceramide synthase in a reconstructed human epidermal keratinization model. *PLoS ONE* **2021**, *16*, e0248150. https://doi.org/10.1371/journal.pone.0248150. PMID: 33684145; PMCID: PMC7939263.
34. Awad, A.B.; Fink, C.S.; Trautwein, E.A.; Ntanios, F.Y. beta-Sitosterol stimulates ceramide metabolism in differentiated Caco2 cells. *J. Nutr. Biochem.* **2005**, *16*, 650–655. https://doi.org/10.1016/j.jnutbio.2005.04.004. PMID: 16098730.
35. Tasyriq, M.; Najmuldeen, I.A.; In, L.L.A.; Mohamad, K.; Awang, K.; Hasima, N. 7α-Hydroxy-β-Sitosterol from *Chisocheton tomentosus*Induces Apoptosis via Dysregulation of Cellular Bax/Bcl-2 Ratio and Cell Cycle Arrest by Downregulating ERK1/2 Activation. *Evid.-Based Complement. Altern. Med.* **2012**, *2012*, 765316. https://doi.org/10.1155/2012/765316. PMID: 22997533; PMCID: PMC3446807.
36. Mao, Z.; Shen, X.; Dong, P.; Liu, G.; Pan, S.; Sun, X.; Hu, H.; Pan, L.; Huang, J. Fucosterol exerts antiproliferative effects on human lung cancer cells by inducing apoptosis, cell cycle arrest and targeting of Raf/MEK/ERK signalling pathway. *Phytomedicine* **2019**, *61*, 152809. https://doi.org/10.1016/j.phymed.2018.12.032. PMID: 31035050.
37. Tkach, M.; Rosemblit, C.; A Rivas, M.; Proietti, C.J.; Flaqué, M.C.D.; Mercogliano, M.F.; Beguelin, W.; Maronna, E.; Guzmán, P.; Gercovich, F.G.; et al. p42/p44 MAPK-mediated Stat3Ser727 phosphorylation is required for progestin-induced full activation of Stat3 and breast cancer growth. *Endocr.-Relat. Cancer* **2013**, *20*, 197–212. https://doi.org/10.1530/erc-12-0194. PMID: 23329648.
38. Mebratu, Y.; Tesfaigzi, Y. How ERK1/2 activation controls cell proliferation and cell death: Is subcellular localization the answer? *Cell Cycle* **2009**, *8*, 1168–1175. https://doi.org/10.4161/cc.8.8.8147. PMID: 19282669; PMCID: PMC2728430.
39. Balmanno, K.; Cook, S.J. Tumour cell survival signalling by the ERK1/2 pathway. *Cell Death Differ.* **2009**, *16*, 368–377. https://doi.org/10.1038/cdd.2008.148. PMID: 18846109.
40. Quah, S.Y.; Tan, M.S.; Teh, Y.H.; Stanslas, J. Pharmacological modulation of oncogenic Ras by natural products and their derivatives: Renewed hope in the discovery of novel anti-Ras drugs. *Pharmacol. Ther.* **2016**, *162*, 35–57. https://doi.org/10.1016/j.pharmthera.2016.03.010. PMID: 27016467.
41. Boutros, T.; Chevet, E.; Metrakos, P. Mitogen-activated protein (MAP) kinase/MAP kinase phosphatase regulation: Roles in cell growth, death, and cancer. *Pharmacol. Rev.* **2008**, *60*, 261–310. https://doi.org/10.1124/pr.107.00106. PMID: 18922965.
42. Sun, Y.; Gao, L.; Hou, W.; Wu, J. β-Sitosterol Alleviates Inflammatory Response via Inhibiting the Activation of ERK/p38 and NF-κB Pathways in LPS-Exposed BV2 Cells. *BioMed Res. Int.* **2020**, *2020*, 7532306. https://doi.org/10.1155/2020/7532306. PMID: 32596368; PMCID: PMC7273476.
43. Viatour, P.; Merville, M.-P.; Bours, V.; Chariot, A. Phosphorylation of NF- kappaB and I kappaB proteins: Implications in cancer and inflammation. *Trends Biochem. Sci.* **2005**, *30*, 43–52. https://doi.org/10.1016/j.tibs.2004.11.009. PMID: 15653325.
44. Cao, Z.-Q.; Wang, X.-X.; Lu, L.; Xu, J.-W.; Li, X.-B.; Zhang, G.-R.; Ma, Z.-J.; Shi, A.-C.; Wang, Y.; Song, Y.-J. β-Sitosterol and Gemcitabine Exhibit Synergistic Anti-pancreatic Cancer Activity by Modulating Apoptosis and Inhibiting Epithelial–Mesenchymal Transition by Deactivating Akt/GSK-3β Signaling. *Front. Pharmacol.* **2019**, *9*, 1525. https://doi.org/10.3389/fphar.2018.01525.
45. Marahatha, R.; Gyawali, K.; Sharma, K.; Gyawali, N.; Tandan, P.; Adhikari, A.; Timilsina, G.; Bhattarai, S.; Lamichhane, G.; Acharya, A.; et al. Pharmacologic activities of phytosteroids in inflammatory diseases: Mechanism of action and therapeutic potentials. *Phytother. Res.* **2021**, *35*, 5103–5124. https://doi.org/10.1002/ptr.7138. PMID: 33957012.
46. Gao, J.; Chen, S.; Zhang, L.; Cheng, B.; Xu, A.; Wu, L.; Zhang, X. Evaluation of cytotoxic and apoptotic effects of individual and mixed 7-ketophytosterol oxides on human intestinal carcinoma cells. *J. Agric. Food Chem.* **2015**, *63*, 1035–1041. https://doi.org/10.1021/jf505079v. PMID: 25542134.
47. Ryan, E.; Chopra, J.; McCarthy, F.; Maguire, A.R.; O'Brien, N.M. Qualitative and quantitative comparison of the cytotoxic and apoptotic potential of phytosterol oxidation products with their corresponding cholesterol oxidation products. *Br. J. Nutr.* **2005**, *94*, 443–451. https://doi.org/10.1079/bjn20051500. PMID: 16176617.
48. Aslan, M.; Afşar, E.; Kırımlıoglu, E.; Çeker, T.; Yılmaz, Ç. Antiproliferative Effects of Thymoquinone in MCF-7 Breast and HepG2 Liver Cancer Cells: Possible Role of Ceramide and ER Stress. *Nutr. Cancer* **2021**, *73*, 460–472. https://doi.org/10.1080/01635581.2020.1751216. PMID: 32286088.
49. Aslan, M. Polyunsaturated fatty acid and sphingolipid measurements by tandem mass spectrometry. *Mini-Rev. Org. Chem.* **2021**, *18*, 3–10. https://doi.org/10.2174/1570193x17999200504094901.